Research Square

Preprints are preliminary reports that have not undergone peer review.
They should not be considered conclusive, used to inform clinical practice,
or referenced by the media as validated information.

Clinical application of a novel coronal imbalance restoration technique for global coronal balance reconstruction in adolescent idiopathic scoliosis: a retrospective cohort study

Yankui Liu
Third Affiliated Hospital of Sun Yat-sen University
Pan Zhou
Third Affiliated Hospital of Sun Yat-sen University
Jingxuan Feng
Third Affiliated Hospital of Sun Yat-sen University
Guoliang Sun
Third Affiliated Hospital of Sun Yat-sen University
Xihua Wu
Third Affiliated Hospital of Sun Yat-sen University
Dehua Liao
Third Affiliated Hospital of Sun Yat-sen University
Hao Zheng
Third Affiliated Hospital of Sun Yat-sen University
Zifang Huang
Third Affiliated Hospital of Sun Yat-sen University
Lei He
helei26@mail.sysu.edu.cn
Third Affiliated Hospital of Sun Yat-sen University

Research Article

Keywords: Adolescent idiopathic scoliosis, Coronal balance, Coronal imbalance restoration, Intraoperative fluoroscopy, Posterior spinal fusion

Posted Date: October 14th, 2026

DOI: https://doi.org/10.21203/rs.3.rs-11095986/v1

License: This work is licensed under a Creative Commons Attribution 4.0 International License. Read Full License

Additional Declarations: No competing interests reported.

Abstract

Purpose: To evaluate the clinical efficacy and potential mechanisms of the coronal imbalance restoration (CIR) technique for restoring coronal balance in patients with adolescent idiopathic scoliosis (AIS) undergoing corrective surgery.

Methods: This retrospective cohort study included 42 patients with AIS (33 females and 9 males; median age, 17 years) who underwent posterior correction and fusion between 2020 and 2024. CIR was performed under intraoperative fluoroscopic guidance. Preoperative, intraoperative, immediate postoperative, and follow-up imaging was analyzed to evaluate changes in coronal balance and correction outcomes.

Results: All patients underwent one-stage posterior simultaneous double-rod derotation and fusion. The cohort included Lenke types 1 (n=8), 2 (n=1), 3 (n=12), 5 (n=15), and 6 (n=6). Based on immediate postoperative CBD, 20 patients were balanced (≤20 mm) and 22 were imbalanced (>20 mm). Coronal imbalance was present in 35.71% preoperatively, 2.38% after final intraoperative correction, 52.38% immediately postoperatively, and 2.38% at final follow-up. Thirty-three patients required repeated intraoperative correction; their initial intraoperative imbalance rate was 57.58%, and most achieved balance after CIR-guided correction.

Conclusion: The results support the effectiveness of CIR for correcting coronal deviation and highlight the value of real-time fluoroscopic assessment in guiding correction. CIR may assist precise management of global coronal alignment and distal three-dimensional restoration in AIS surgery.

Introduction

Adolescent idiopathic scoliosis (AIS) is a three-dimensional spinal deformity involving coronal curvature, sagittal profile, and vertebral rotation. It affects approximately 1%–3% of the population, predominantly females [1], with a reported prevalence of 1.23% in China [2] and increasing detection in the United States [3] and Japan [4]. Surgery is generally considered when the Cobb angle exceeds 40° [5]. Correction has evolved from two-dimensional realignment toward three-dimensional reconstruction [6]. Techniques including global rod derotation [7], direct vertebral rotation [8], simultaneous double-rod rotation [9], vertebral coplanar alignment [10], and dual rod translation [11] have improved axial and apical correction. However, these methods mainly address the instrumented curve, while global coronal balance is often assessed only after surgery.

Postoperative coronal imbalance (CIB) remains a clinically important challenge and occurs in approximately 20%–30% of patients with AIS [12–15]. CIB is commonly defined as a coronal balance distance (CBD), measured between the C7 plumb line and central sacral vertical line (CSVL), greater than 20 mm. It has been associated with poorer outcomes, pain, and revision surgery [16]. An intraoperative strategy that directly addresses coronal shift before final fixation may therefore be valuable.

We developed the coronal imbalance restoration (CIR) technique to actively counteract coronal deviation. Opposing horizontal forces are applied proximally and distally to recenter the C7 plumb line over the CSVL before final fixation. The maneuver is adjusted iteratively under fluoroscopic guidance. In addition to global recentering, CIR may improve distal three-dimensional parameters, including LIV tilt, LIV translation, and AVT. This study evaluated CIR in patients with AIS undergoing posterior spinal fusion by tracking CBD at five perioperative time points and comparing patients with and without immediate postoperative balance. We also assessed CBD, SVA, LIV-CSVL distance, LIV rotation, and AVT.

Methods

- This retrospective cohort study was conducted in accordance with the Declaration of Helsinki. Written informed consent was obtained from all patients and their legal guardians.

Table 1
Baseline Characteristics of the Patients

Characteristic	Value
Age, years	17 (13–25)
Sex	Female: 33 (78.57%)
	Male: 9 (21.43%)
Follow-up, months	9 (6, 12)
Operative time, min	402.5 (302.2, 483.8)
Blood loss, mL	829.4 ± 361.2
Postoperative LIV	L2: 8 (19.05%)
	L3: 13 (30.95%)
	L4: 17 (40.48%)
	L5: 4 (9.52%)
Lenke classification	Type 1: 8 (19.05%)
	Type 2: 1 (2.38%)
	Type 3: 12 (28.57%)
	Type 5: 15 (35.71%)
	Type 6: 6 (14.29%)

Inclusion criteria were a diagnosis of AIS, complete perioperative radiographic data, and use of CIR. Patients with congenital or neuromuscular scoliosis, severe comorbidities, neurological deficits, or incomplete imaging or follow-up data were excluded.

Patients were grouped by immediate postoperative CBD as balanced (≤ 20 mm, n = 20) or imbalanced (> 20 mm, n = 22). All underwent posterior spinal fusion with CIR and intraoperative fluoroscopic assessment.

Data Collection. Radiographic data were collected preoperatively, intraoperatively, immediately postoperatively, and at final follow-up. Standing full-spine radiographs, computed tomography (CT), and intraoperative fluoroscopy were assessed. Demographic and operative data were also recorded.

Radiographic Parameter Measurement. Measurements were obtained from standing anteroposterior and lateral full-spine radiographs. The main and compensatory Cobb angles were defined by the intersecting lines drawn along the superior endplate of the upper end vertebra and the inferior endplate of the lower end vertebra. The sagittal vertical axis (SVA) was the horizontal distance from the C7 plumb line to the posterosuperior corner of S1; apical vertebral translation (AVT) was the horizontal distance from the geometric center of the apical vertebra to the central sacral vertical line (CSVL); and coronal balance distance (CBD) was the horizontal distance between the C7 plumb line and the CSVL. Coronal imbalance was defined as CBD > 20 mm. CBD was measured preoperatively, after the first intraoperative correction, after the final intraoperative correction, immediately postoperatively, and at final follow-up.

LIV-related parameters included LIV tilt, LIV–CSVL distance, and LIV rotation. LIV tilt was the angle between the inferior endplate of the LIV and the horizontal line; LIV–CSVL distance was the horizontal distance from the geometric center of the LIV to the CSVL; and LIV rotation was measured on axial CT as the angle between the anteroposterior axis of the LIV and the midsagittal line of the body. L5 tilt was the angle between the inferior endplate of L5 and the horizontal line. The stable vertebra (SV) was defined as the lowest vertebra most closely bisected by the CSVL. LIV–SV was expressed as the difference in vertebral levels and assigned a negative value when the LIV was cranial to the SV. LIV rotation was measured on CT; all other parameters were measured on standing full-spine radiographs.

Correction rates were calculated using the following formulas:

$$\text{Postoperative correction rate} = \frac{\text{Preoperative Cobb angle} - \text{Postoperative Cobb angle}}{\text{Preoperative Cobb angle}}$$

$$\text{Final follow-up correction rate} = \frac{\text{Preoperative Cobb angle} - \text{Final follow-up Cobb angle}}{\text{Preoperative Cobb angle}}$$

Postoperative LIV tilt correction rate = $\frac{\text{Preoperative LIV tilt}-\text{Postopreative LIV tilt}}{\text{Preoperative LIV tilt}}$

Final follow-up LIV tilt correction rate = $\frac{\text{Preoperative LIV tilt}-\text{Final follow}-\text{up LIV tilt}}{\text{Preoperative LIV tilt}}$

Postoperative LIV-CSVL correction rate = $\frac{\text{Preoperative LIV}-\text{CSVL}-\text{Postoperative LIV}-\text{CSVL}}{\text{Preoperative LIV}-\text{CSVL}}$

Final follow-up LIV-CSVL correction rate = $\frac{\text{Preoperative LIV}-\text{CSVL}-\text{Final follow}-\text{up LIV}-\text{CSVL}}{\text{Preoperative LIV}-\text{CSVL}}$

Postoperative AVT correction rate = $\frac{\text{Preoperative AVT}-\text{Postopreative AVT}}{\text{Preoperative AVT}}$

Final follow-up AVT correction rate = $\frac{\text{Preoperative AVT}-\text{Final follow}-\text{up AVT}}{\text{Preoperative AVT}}$

All procedures were performed by the same experienced spine surgeon. After induction of general anesthesia and initiation of neurophysiological monitoring, patients were positioned prone on a radiolucent operating table. The UIV, LIV, and fusion range were preliminarily estimated from standing radiographs. After placement of localization screws, the final LIV was selected according to three criteria: (1) it was the most cranial vertebra touched by the CSVL; (2) vertebral rotation was less than grade II according to the Nash–Moe classification; and (3) the LIV tilt angle was < 25°. A candidate vertebra was accepted only when all three criteria were met, and the most cranial acceptable vertebra was selected as the final LIV to preserve as many distal lumbar motion segments as possible (Fig. 1A).

Pedicle screws were inserted at the planned levels (Fig. 1B), and contoured bilateral rods were seated. After provisional fixation, distal compression and distraction were applied to reduce LIV tilt and compensatory translation (Fig. 1C).

CIR was then performed by applying a transverse force toward the midline proximally and an opposing force distally. These forces translated the instrumented spine while limiting en bloc displacement. Distal compression and distraction were adjusted to reduce LIV tilt and restore coronal alignment (Fig. 1D). Rod derotation, segmental translation, compression, distraction, and in situ bending were added as needed.

After satisfactory correction, all set screws were tightened and final alignment was assessed (Fig. 1E). Fluoroscopy confirmed screw position, implant configuration, coronal balance, and LIV orientation. Posterior fusion was completed with autologous and allogeneic bone graft.

Statistical Analysis. Analyses were performed using R and IBM SPSS Statistics. Normality was assessed with the Shapiro–Wilk test. Normally distributed continuous variables are presented as mean ± standard deviation, non-normally distributed variables as median (Q1, Q3), and categorical variables as counts and percentages. Between-group continuous variables were compared using Welch's t test or the Wilcoxon rank-sum test, as appropriate, and categorical variables using Fisher's exact test. Within-patient comparisons across three time points used repeated-measures analysis of variance with the Greenhouse–Geisser correction or the Friedman test, followed by post hoc pairwise comparisons; two-time-point comparisons used paired t tests or Wilcoxon signed-rank tests. Overall CBD across five time points was compared using the Friedman test. All tests were two-sided, and $P < 0.05$ was considered statistically significant.

Schematic illustration of the coronal imbalance restoration (CIR) technique. (A) Coronal deformity before corrective manipulation. (B) Pedicle screw placement at the predetermined instrumented levels. (C) Differential compression and distraction are applied to lower the relatively elevated side and elevate the relatively depressed side, thereby leveling the tilted vertebrae and reducing lower instrumented vertebra tilt. (D) The surgeon manually applies oppositely directed horizontal pushing forces to the proximal and distal portions of the patient's trunk. These counteracting forces reposition the trunk and instrumented spine toward the coronal midline, while compression and distraction are adjusted as required to maintain vertebral horizontalization. (E) Final coronal alignment after completion of correction and definitive fixation. Green arrows indicate the directions of the corrective forces; gray arrows indicate the procedural sequence. CIR, coronal imbalance restoration.

Results

General Characteristics.

Patients were classified as balanced (n = 20) or imbalanced (n = 22) by immediate postoperative CBD. The groups did not differ significantly in age, sex, preoperative LIV, Lenke type, LIV-SV, follow-up, operative time, or blood loss. Postoperative LIV distribution

differed between groups (P = 0.0239): L4 was most common in the imbalanced group, whereas L3 was most common in the balanced group (Table 1 and Table 3).

Analysis of Coronal Balance Data.

Radiographs were assessed preoperatively, intraoperatively, postoperatively, and at final follow-up. CIR was repeated when fluoroscopy showed insufficient correction of coronal alignment or vertebral rotation. Thirty-three patients required repeated correction, while 9 achieved satisfactory correction after one application.

Preoperative CBD was 14.50 mm (Q1–Q3, 6.10–20.34 mm). Among the 33 patients requiring repeated correction, CBD was 21.90 mm (0.00–43.32 mm) after the first intraoperative correction and decreased to 8.57 mm (0.00–15.47 mm) after the final intraoperative correction (P = 0.067 vs. preoperative). Immediate postoperative CBD was 18.00 mm (12.31–30.87 mm), higher than both the preoperative value (P = 0.029) and the final intraoperative value (P < 0.001). At final follow-up, CBD decreased to 7.00 mm (0.00–11.35 mm), lower than the immediate postoperative (P < 0.001) and preoperative values (P = 0.013), with no difference from the final intraoperative value (P = 0.508). The coronal imbalance rate changed from 35.71% (15/42) preoperatively to 57.58% (19/33) after the first intraoperative correction, 2.38% (1/42) after the final intraoperative correction, 52.38% (22/42) immediately postoperatively, and 2.38% (1/42) at final follow-up. Figure 2 illustrates the dynamic change in CBD and recovery of coronal balance across the five time points through both group distributions and individual longitudinal trajectories (Fig. 2; Table 2).

a

Figure 2 Dynamic changes in CBD across different time points.(a) Box-and-whisker plots showing the distribution of CBD values at the preoperative, first intraoperative, final intraoperative, immediate postoperative, and final follow-up time points. Individual data points are superimposed.(b) Spaghetti plot illustrating longitudinal CBD changes in individual patients across the five time points, demonstrating the temporal pattern of coronal balance restoration from preoperative assessment to final follow-up.

Table 2
Coronal Balance Distance and Coronal Imbalance Rates at Different Time Points

Time point	CBD, median (Q1, Q3), mm	Imbalance, n/N (%)	P vs. preoperative	P vs. first intraoperative	P vs. final intraoperative	P vs. postoperative	P vs. follow-up
Preoperative	14.50 (6.10, 20.34)	15/42 (35.71)	—	—	—	—	—
First intraoperative	21.90 (0.00, 43.32)	19/33 (57.58)	0.052	—	—	—	—
Final intraoperative	8.57 (0.00, 15.47)	1/42 (2.38)	0.067	< 0.001	—	—	—
Postoperative	18.00 (12.31, 30.87)	22/42 (52.38)	0.029	0.815	< 0.001	—	—
Final follow-up	7.00 (0.00, 11.35)	1/42 (2.38)	0.013	< 0.001	0.508	< 0.001	—

Comparison of Correction Outcomes Between Groups

Coronal and Sagittal Plane Correction.No statistically significant differences were found between the imbalanced and balanced groups regarding the main curve and minor curve angles preoperatively, immediately postoperatively, or at follow-up, nor in their respective correction rates postoperatively and at follow-up (P > 0.05). The postoperative CBD was significantly higher in the imbalanced group compared to the balanced group (31.27 [IQR: 14.27] mm vs. 11.28 ± 5.68 mm, P < 0.0001). However, no statistically significant differences were noted between the two groups in preoperative CBD (imbalanced: 17.22 ± 10.92 mm vs. balanced: 13.87 ± 8.7 mm, P = 0.2813) or final follow-up CBD (imbalanced: 8.3 ± 6.32 mm vs. balanced: 5.98 [IQR: 10.03] mm, P = 0.2177). Furthermore, there were no statistically significant differences in SVA between the groups preoperatively, postoperatively, or at the final follow-up (P > 0.05).

Comparison of LIV-related and Other Radiographic Parameters. No statistically significant differences were observed between the two groups in LIV tilt preoperatively or at the final follow-up, nor in the final follow-up LIV tilt correction rate (P > 0.05). However, the postoperative LIV tilt correction rate was lower in the imbalanced group compared to the balanced group (imbalanced: 0.67 [IQR: 0.5] vs. balanced: 0.89 [IQR: 0.32], P = 0.282), and although the postoperative LIV tilt was higher in the imbalanced group, the difference was not statistically significant (imbalanced: 6.59° ± 5.26° vs. balanced: 2.22° [IQR: 6.18°], P = 0.0558). There were no statistically significant differences between the groups regarding LIV-CSVL distance and its associated correction rates at any time point (P > 0.05), nor in preoperative or postoperative LIV rotation (P > 0.05). While preoperative AVT, final follow-up AVT, and final follow-up AVT correction rate showed no statistically significant differences between the groups (P > 0.05), the imbalanced group exhibited a significantly higher postoperative AVT (19.86 ± 11.11 mm vs. 13.27 ± 8.48 mm, P = 0.0380) and a correspondingly lower postoperative AVT correction rate (0.59 [IQR: 0.18] vs. 0.75 ± 0.15, P = 0.0126). Additionally, L5 tilt showed no statistically significant differences between the groups preoperatively, postoperatively, or at the final follow-up (P > 0.05). These between-group comparisons are summarized in Table 3.

Table 3
Comparison of Baseline Characteristics Between the Postoperative Coronal Balance and Imbalance Groups

Variable	Postoperative coronal balance group (n = 20)	Postoperative coronal imbalance group (n = 22)	P value
Age, years	19.5 (12.8, 25.0)	15.5 (13.2, 22.5)	0.6677
Sex	Female: 18 (90%)	Female: 15 (68.18%)	0.1349
	Male: 2 (10%)	Male: 7 (31.82%)	
Preoperative LIV	L2: 3 (15%)	L2: 1 (4.55%)	0.2162
	L3: 3 (15%)	L3: 1 (4.55%)	
	L4: 9 (45%)	L4: 8 (36.36%)	
	L5: 5 (25%)	L5: 12 (54.55%)	
Postoperative LIV	L2: 4 (20%)	L2: 4 (18.18%)	0.0239
	L3: 10 (50%)	L3: 3 (13.64%)	
	L4: 6 (30%)	L4: 11 (50%)	
	L5: 0 (0%)	L5: 4 (18.18%)	
Preoperative LIV–SV	-1 (-1, 0)	0 (-1, 0)	0.1141
Postoperative LIV–SV	-2 (-2, -1)	-1 (-2, -1)	0.2218
Lenke classification	Type 1: 7 (35%)	Type 1: 1 (4.55%)	0.0765
	Type 2: 1 (5%)	Type 2: 0 (0%)	
	Type 3: 5 (25%)	Type 3: 7 (31.82%)	
	Type 5: 5 (25%)	Type 5: 10 (45.45%)	
	Type 6: 2 (10%)	Type 6: 4 (18.18%)	
Follow-up, months	9.5 (6.0, 12.0)	8.5 (6.0, 12.0)	0.7697
Operative time, min	402.5 (292.2, 458.0)	401.5 (318.0, 527.2)	0.6233
Blood loss, mL	685 (500, 1050)	800 (643.8, 1175)	0.3501

Overall Cohort Analysis

Coronal Plane Correction. Radiographic parameters were compared preoperatively, postoperatively, and at final follow-up in the 42 patients.

The main-curve Cobb angle decreased from 56.94° (IQR, 25.12°) preoperatively to 7.47° (10.18°) postoperatively and 7.32° (12.27°) at final follow-up (both P < 0.001 vs. preoperative), with no difference between postoperative and follow-up measurements (P = 0.743). Postoperative and follow-up main-curve correction rates were 84.96% ± 12.01% and 84.27% ± 12.30%, respectively (P = 0.630). The compensatory curve decreased from 48.74° ± 13.07° preoperatively to 8.26° ± 4.94° postoperatively and 7.63° ± 4.22° at follow-up (both P < 0.001 vs. preoperative), with no postoperative-to-follow-up difference. SVA did not differ across the three time points (P = 0.792). AVT

decreased from 59.01 ± 20.43 mm preoperatively to 16.72 ± 10.38 mm postoperatively and 12.57 ± 8.29 mm at follow-up (both P < 0.001 vs. preoperative; postoperative vs. follow-up, P = 0.003); the corresponding correction rates were 69.00% ± 16.84% and 76.85% ± 15.92% (P = 0.002).

Correction of LIV-related and Other Radiographic Parameters. The median LIV tilt decreased from 22.00° (IQR: 16.67°) preoperatively to 5.12° (IQR: 8.00°) postoperatively (P < 0.001) and was maintained at 3.00° (IQR: 6.49°) at the final follow-up (P < 0.001 vs. preoperative; P = 0.326 vs. postoperative). This was reflected in the LIV tilt correction rates (postoperative: 76.36% [IQR: 53.48%] vs. follow-up: 87.56% [IQR: 34.41%], P = 0.027). Similarly, the median LIV-CSVL distance improved from 18.54 (IQR: 11.54) mm preoperatively to 6.06 (IQR: 9.00) mm postoperatively (P < 0.001), remaining stable at 6.83 (IQR: 9.10) mm at follow-up (P < 0.001 vs. preoperative; P = 0.513 vs. postoperative). There was no statistically significant difference between the postoperative and follow-up LIV-CSVL correction rates (66.70% [IQR: 53.78%] vs. 66.77% [IQR: 40.94%], P = 0.561). Furthermore, the mean LIV rotation decreased significantly from 10.94° ± 4.45° preoperatively to 5.88° ± 3.58° postoperatively (P < 0.001). The median L5 tilt improved from 12.00° (IQR: 9.89°) preoperatively to 4.32° (IQR: 6.21°) postoperatively (P < 0.001) and reached 3.00° (IQR: 5.99°) at follow-up (P < 0.001 vs. preoperative; P = 0.081 vs. postoperative). Finally, our results indicate that, guided by intraoperative fluoroscopy, the ultimately fused LIV was situated approximately 1.38 ± 0.79 segments cranial to the SV, meaning it was selected more proximally than the LIV initially determined from preoperative standing radiographs (vs. preoperative LIV-SV: -0.67 ± 0.69, P < 0.001). Complete radiographic comparisons across time points are presented in Table 4. Representative perioperative imaging sequences demonstrating CIR-guided balance restoration and distal correction are shown in Figs. 3 and 4.

Table 4
Comparison of Radiographic Parameters at Different Time Points

Main curve (°)	Preoperative	Postoperative	Follow-up	Statistic	P value	Preoperative vs. postoperative	Preoperative vs. follow-up	Postoperative vs. follow-up
	56.94 (25.12)	**7.47 (10.18)**	**7.32 (12.27)**	**χ^2=64.255**	**< 0.001**	**P < 0.001**	**P < 0.001**	**P = 0.743**
Main-curve correction rate (%)		84.96 ± 12.01	84.27 ± 12.30	t = 0.486	0.630			
Compensatory curve (°)	48.74 ± 13.07	8.26 ± 4.94	7.63 ± 4.22	F = 270.431	< 0.001	P < 0.001	P < 0.001	P = 1.000
Compensatory-curve correction rate (%)		83.68 ± 8.27	84.71 ± 7.83	t=-0.506	0.619			
Sagittal vertical axis (SVA, mm)	13.05 (5.75, 28.00)	19.84 (9.91, 39.11)	14.07 (8.00, 28.00)	χ^2=0.467	0.792			
LIV tilt (°)	22.00 (16.67)	5.12 (8.00)	3.00 (6.49)	χ^2=69.329	< 0.001	P < 0.001	P < 0.001	P = 0.326
LIV-tilt correction rate (%)		76.36 (53.48)	87.56 (34.41)	W = 320.00	0.027			
LIV–CSVL distance (mm)	18.54 (11.54)	6.06 (9.00)	6.83 (9.10)	χ^2=46.105	< 0.001	P < 0.001	P < 0.001	P = 0.513
LIV–CSVL correction rate (%)		66.70 (53.78)	66.77 (40.94)	W = 294.00	0.561			
LIV rotation (°)	10.94 ± 4.45	5.88 ± 3.58		t = 6.344	< 0.001			
Apical vertebral translation (AVT, mm)	59.01 ± 20.43	16.72 ± 10.38	12.57 ± 8.29	F = 181.486	< 0.001	P < 0.001	P < 0.001	P = 0.003
AVT correction rate (%)		69.00 ± 16.84	76.85 ± 15.92	t=-3.402	0.002			
L5 tilt (°)	12.00 (9.89)	4.32 (6.21)	3.00 (5.99)	χ^2=40.096	< 0.001	P < 0.001	P < 0.001	P = 0.081
LIV–SV	-0.67 ± 0.69	-1.38 ± 0.79		Z=-4.973	< 0.001			

Discussion

CIR achieved stable radiographic correction in posterior fusion for AIS. At final follow-up, the main-curve correction rate was approximately 84%, median CBD was 7.00 mm, and coronal imbalance decreased from 35.71% preoperatively to 2.38%. These findings suggest that adding an active maneuver directed at global coronal displacement to conventional three-dimensional correction allows curve correction and trunk recentering to be evaluated concurrently during surgery. No coronal decompensation requiring revision or severe technique-related complication was observed during follow-up; however, safety conclusions should remain cautious because of the small sample and short follow-up.

CIR extends the correction target from Cobb-angle reduction alone to global coronal balance. By applying opposing horizontal forces proximally and distally, together with distal compression, distraction, and rod adjustment, the surgeon can repeatedly assess the relationship between the C7 plumb line and CSVL before final locking. Concurrent improvements in AVT, LIV tilt, LIV–CSVL distance, and LIV rotation suggest that trunk recentering may be associated with coordinated restoration of distal coronal and axial alignment. Previous

studies have likewise identified LIV tilt, translation, and its relationship to the CSVL as important determinants of postoperative coronal balance [17–20].

A notable finding was that the imbalance rate was only 2.38% on final intraoperative fluoroscopy, increased to 52.38% on immediate postoperative standing radiographs, and then decreased to 2.38% at follow-up. Prone fluoroscopy under general anesthesia without axial loading is not directly equivalent to postoperative standing balance. Early pain, muscle spasm, protective posture, and incomplete pelvic and trunk compensation may explain this discrepancy. Therefore, immediate postoperative CBD > 20 mm does not necessarily indicate fixation failure and should be interpreted together with distal vertebral alignment, the direction of balance change, and the follow-up trajectory. This interpretation is consistent with previous reports of spontaneous recovery in some patients [12, 21, 22], although persistent imbalance may be associated with poorer clinical outcomes [15, 22].

Intraoperative fluoroscopy also provided dynamic information for final LIV selection. The final LIV was, on average, 1.38 levels cranial to the preoperatively estimated SV, suggesting that extension to a more distal lumbar level may be avoided in some patients once acceptable distal alignment and coronal balance have been achieved [12, 21–23]. This finding has potential clinical relevance for preserving lumbar motion segments; however, because this study lacked a control group without CIR or without fluoroscopy-guided LIV selection, it cannot establish that CIR itself necessarily reduces the number of fused levels.

This study has several limitations. First, its retrospective single-center design, small sample, and short follow-up may have introduced selection bias and limit both generalizability and assessment of long-term safety. Second, no control group was treated without CIR or without fluoroscopy-guided LIV selection; therefore, the observed correction and preservation of fusion levels cannot be attributed directly to CIR. In addition, the different loading conditions between intraoperative prone fluoroscopy and postoperative standing radiographs limit direct comparison of CBD across time points. Patient-reported outcomes such as SRS-22 were unavailable, and interobserver and intraobserver reliability of the radiographic measurements requires further validation. Prospective multicenter controlled studies using standardized imaging protocols, blinded measurements, longer follow-up, and clinical outcomes are needed to confirm the durability and safety of CIR.

Conclusion

Overall, CIR appears to be a safe, feasible, and potentially valuable strategy for coronal balance reconstruction in AIS. Real-time assessment and repeated correction may improve global alignment and distal three-dimensional restoration while preserving compensatory capacity. Although immediate postoperative imbalance was common, most patients recovered balance during follow-up. Larger multicenter studies with longer follow-up and clinical outcomes are warranted.

Declarations

Ethics approval and consent to participate

This retrospective cohort study was conducted in accordance with the Declaration of Helsinki and was approved by the Medical Ethics Committee of the Third Affiliated Hospital of Sun Yat-sen University (approval No. II2025-118-01; approved on 31 March 2025). Written informed consent was obtained from all patients and their legal guardians.

Consent for publication

Agree.

Availability of data and materials

The data that support the findings of this study are available from the corresponding author on reasonable request, subject to institutional approval and applicable privacy restrictions. Because the dataset contains clinical and radiographic information from human participants, it is not publicly available.

Competing interests

The authors have nothing to disclose.

Funding

This work was supported by the “Yuanhang Program” of the Clinical Research Special Fund of the Third Affiliated Hospital of Sun Yat-sen University, China (Grant No. YHJH202405).

Authors’ contributions

YL, ZH, and LH conceptualized the study. YL, JF, XW, ZH, and LH developed the methodology. YL, PZ, GS, DL, and HZ curated the data, while PZ, JF, and HZ performed the formal analyses. YL, PZ, and JF conducted the visualization and drafted the original manuscript. ZH and LH administered the project, and LH secured funding. All authors critically reviewed and edited the manuscript and approved the final version.

Acknowledgements

None.

References

1. Wang S, Li M, Ren J, et al. Global prevalence and associated risk factors of scoliosis in children and adolescents: A systematic review and meta-analysis. BMC Public Health. 2025;25. https://doi.org/10.1186/s12889-025-24905-4.
2. Tu Q, Xu W, Feng Y, et al. Prevalence and determinants of adolescent idiopathic scoliosis from school screening in xiaoshan district, hangzhou, China. Front Public Health. 2025;13. https://doi.org/10.3389/fpubh.2025.1595793.
3. Sanghvi PA, Burkhart RJ, Abid R, et al. Epidemiological trends and projections of adolescent idiopathic scoliosis patients among 118 thousand patients. J Am Acad Orthop Surg. 2026. https://doi.org/10.5435/JAAOS-D-25-00893.
4. Morino T, Murakami Y, Kinoshita T, et al. Trends in the prevalence of adolescent idiopathic scoliosis in a japanese prefecture: A 25-year population-based school screening study using moiré topography. Global Spine J. 2026;21925682261417283. https://doi.org/10.1177/21925682261417283.
5. Negrini S, Donzelli S, Aulisa AG, et al. 2016 SOSORT guidelines: Orthopaedic and rehabilitation treatment of idiopathic scoliosis during growth. Scoliosis Spinal Disord. 2018;13:3. https://doi.org/10.1186/s13013-017-0145-8.
6. Jain A, Ahuja K, Roberts SB, Tsirikos AI. Techniques of deformity correction in adolescent idiopathic scoliosis—a narrative review of the existing literature. J Clin Med. 2025;14:2396. https://doi.org/10.3390/jcm14072396.
7. Anekstein Y, Mirovsky Y, Arnabitsky V, et al. Reversing the concept: Correction of adolescent idiopathic scoliosis using the convex rod de-rotation maneuver. Eur Spine J. 2012;21:1942–9. https://doi.org/10.1007/s00586-012-2355-3.
8. Kim HJ, Chang D-G, Lenke LG, et al. Rotational changes following use of direct vertebral rotation in adolescent idiopathic scoliosis: A long-term radiographic and computed tomography evaluation. Spine. 2024;49:1059–68. https://doi.org/10.1097/BRS.0000000000004869.
9. Sudo H, Ito M, Abe Y, et al. Surgical treatment of lenke 1 thoracic adolescent idiopathic scoliosis with maintenance of kyphosis using the simultaneous double-rod rotation technique. Spine. 2014;39:1163–9. https://doi.org/10.1097/BRS.0000000000000364.
10. Vallespir GP, Flores JB, Trigueros IS, et al. Vertebral coplanar alignment: A standardized technique for three dimensional correction in scoliosis surgery: technical description and preliminary results in lenke type 1 curves. Spine. 2008;33:1588–97. https://doi.org/10.1097/BRS.0b013e3181788704.
11. Hori Y, Namikawa T, Kawamura M, et al. Posterior spinal fusion using dual rod translation: Impact on kyphosis restoration in AIS. Eur Spine J. 2026. https://doi.org/10.1007/s00586-025-09695-y.
12. Matsumura A, Iwamae M, Namikawa T, et al. Spontaneous improvement of postoperative coronal imbalance following selective thoracolumbar-lumbar fusion in lenke 5C adolescent idiopathic scoliosis. World Neurosurg. 2021;151:e241–9. https://doi.org/10.1016/j.wneu.2021.04.024.
13. Ohrt-Nissen S, Cheung PWH, Kawasaki S, et al. Curve overcorrection predicts coronal imbalance in selective thoracic fusion in adolescent idiopathic scoliosis. Global Spine J. 2024;14:856–61. https://doi.org/10.1177/21925682221124526.
14. Qiao H, Yan K, Liao B. Risk of coronal imbalance after posterior surgery for adolescent idiopathic scoliosis of type Lenke5C. Curr Med Res Opin. 2024;40:1785–91. https://doi.org/10.1080/03007995.2024.2391556.
15. Fang Y, Li J, Hu Z, et al. Postoperative coronal imbalance in lenke 5C adolescent idiopathic scoliosis: Evolution, risk factors, and clinical implications. Neurospine. 2024;21:903–12. https://doi.org/10.14245/ns.2448544.272.
16. Banno T, Yamato Y, Oba H, et al. Risk factors and clinical impact of persistent coronal imbalance after posterior spinal fusion in thoracolumbar/lumbar idiopathic scoliosis. J Neurosurgery: Spine. 2022;37:883–92. https://doi.org/10.3171/2022.5.SPINE22385.

17. Li J, Hwang SW, Shi Z, et al. Analysis of radiographic parameters relevant to the lowest instrumented vertebrae and postoperative coronal balance in lenke 5C patients. Spine. 2011;36:1673–8. https://doi.org/10.1097/BRS.0b013e3182091fba.
18. Yang X, Hu B, Song Y, et al. Coronal and sagittal balance in lenke 5 AIS patients following posterior fusion: Important role of the lowest instrument vertebrae selection. BMC Musculoskelet Disord. 2018;19:212. https://doi.org/10.1186/s12891-018-2135-2.
19. Zhuang Q, Zhang J, Wang S, et al. How to select the lowest instrumented vertebra in lenke type 5 adolescent idiopathic scoliosis patients? Spine J. 2021;21:141–9. https://doi.org/10.1016/j.spinee.2020.08.006.
20. Yamada K, Sudo H, Abe Y, et al. Influence of lateral translation of lowest instrumented vertebra on L4 tilt and coronal balance for thoracolumbar and lumbar curves in adolescent idiopathic scoliosis. J Clin Med. 2023;12:1389. https://doi.org/10.3390/jcm12041389.
21. Hwang CJ, Lee CS, Kim H, et al. Spontaneous correction of coronal imbalance after selective thoracolumbar-lumbar fusion in patients with lenke-5C adolescent idiopathic scoliosis. Spine J. 2018;18:1822–8. https://doi.org/10.1016/j.spinee.2018.03.013.
22. Mannem A, Cheung PWH, Kawasaki S, et al. What determines immediate postoperative coronal balance and delayed global coronal balance after anterior spinal fusion for lenke 5C curves? Eur Spine J. 2021;30:2007–19. https://doi.org/10.1007/s00586-021-06807-2.
23. Mai L, Liu Y, Zhu R, et al. The impact of intraoperative prone lumbar fluoroscopy under anesthesia on the selection of lowest instrumented vertebra and surgical outcomes in adolescent idiopathic scoliosis with lumbar structural curves. BMC Musculoskelet Disord. 2025;26:739. https://doi.org/10.1186/s12891-025-08974-5.

Figures

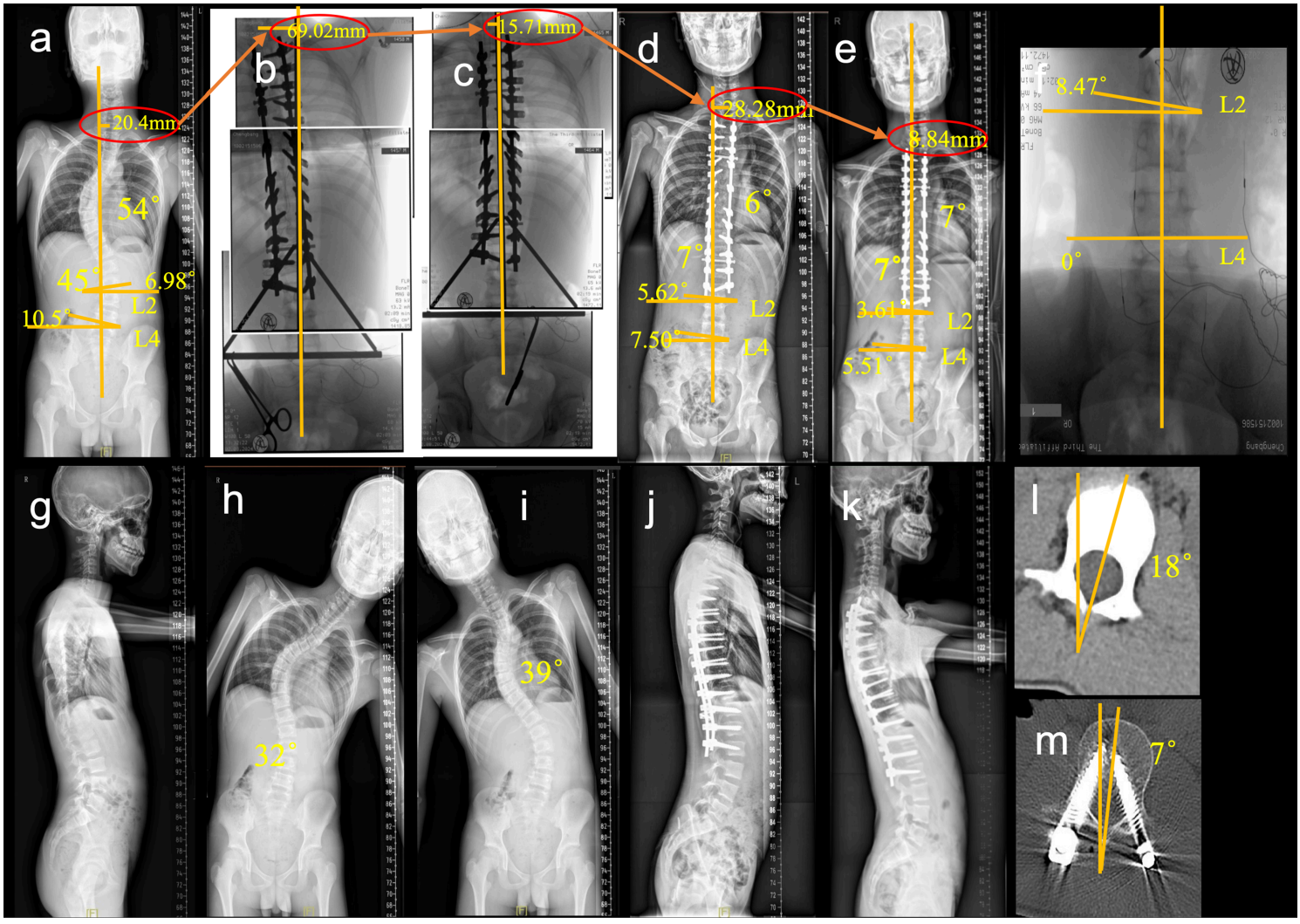


Figure 3

Typical radiographic presentation of a 12-year-old male patient with Lenke type 3 AIS treated using the CIR technique. (a) Preoperative standing full-spine AP radiograph showing a CBD of 20.4 mm, main and minor curve Cobb angles of 54° and 45°, and L2 and L4 tilt angles of 6.98° and 10.5°, respectively. (b, c) Initial and final intraoperative fluoroscopic images showing an improvement in CBD from 69.02 mm to 15.71 mm after CIR correction. (d) Immediate postoperative AP radiograph showing a CBD of 28.28 mm, main and minor curve Cobb angles of 6° and 7°, and L2 and L4 tilt angles of 5.62° and 7.50°, respectively. (e) AP radiograph at the 12-month follow-up showing a CBD of 8.84 mm, main and minor curve Cobb angles of 7° and 7°, and L2 and L4 tilt angles of 3.61° and 5.51°, respectively. (f) Intraoperative AP pelvic fluoroscopy for LIV selection. The L2 and L4 tilt angles were 8.47° and 0°, respectively. L2 was selected as the final LIV instead of the preoperatively planned L4, preserving two distal lumbar motion segments. (g) Preoperative standing full-spine lateral radiograph. (h, i) Left and right bending radiographs showing Cobb angles of 32° and 39°, respectively. (j, k) Immediate postoperative and final follow-up lateral radiographs. (l, m) Preoperative and postoperative axial CT images at L2 showing an improvement in LIV rotation from 18° to 7°.

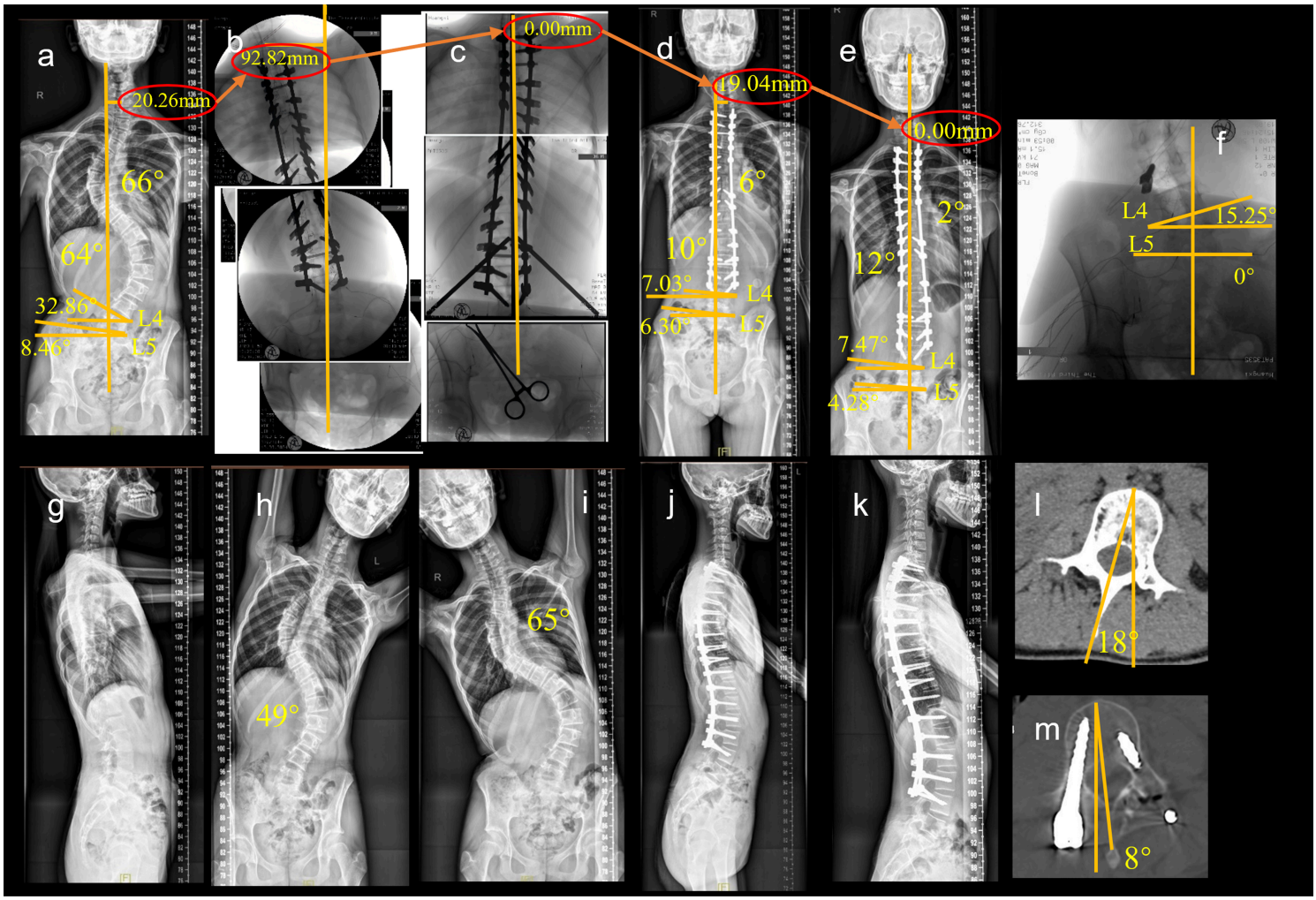


Figure 4

Typical radiographic presentation of a 12-year-old female patient with Lenke type 3 AIS treated using the CIR technique. (a) Preoperative standing full-spine AP radiograph showing a CBD of 20.26 mm, main and minor curve Cobb angles of 66° and 64°, and L4 and L5 tilt angles of 32.86° and 8.46°, respectively. (b, c) Initial and final intraoperative fluoroscopic images showing an improvement in CBD from 92.82 mm to 0 mm after CIR correction. (d) Immediate postoperative AP radiograph showing a CBD of 19.04 mm, main and minor curve Cobb angles of 6° and 10°, and L4 and L5 tilt angles of 7.03° and 6.30°, respectively. (e) AP radiograph at the 10-month follow-up showing a CBD of 0 mm, main and minor curve Cobb angles of 2° and 12°, and L4 and L5 tilt angles of 7.47° and 4.28°, respectively. (f) Intraoperative AP pelvic fluoroscopy for LIV selection. The L4 and L5 tilt angles were 15.25° and 0°, respectively. L4 was selected as the final LIV instead of the preoperatively planned L5, preserving one distal lumbar motion segment. (g) Preoperative standing full-spine lateral radiograph. (h, i) Left and right bending radiographs showing Cobb angles of 49° and 65°, respectively. (j, k) Immediate postoperative and final follow-up lateral radiographs. (l, m) Preoperative and postoperative axial CT images at L4 showing an improvement in LIV rotation from 18° to 8°.

Supplementary Files

This is a list of supplementary files associated with this preprint. Click to download.

- Table1V4.docx
- Table2V4.docx
- Table3V4.docx
- Table4V4.docx